A Solution-Processed Trilayer Electrochemical Device: Localizing the Light Emission for Optimized Performance

Shi Tang,[†] Andreas Sandström,[†] Junfeng Fang,[‡] and Ludvig Edman*,[†]

[†]The Organic Photonics and Electronics Group, Umeå University, SE-901 87 Umeå, Sweden

[‡]Ningbo Institute of Materials Technology and Engineering, Chinese Academy of Sciences, Ningbo, 315211 Zhejiang, People's Republic of China

S *Supporting Information*

ABSTRACT: We present a solution-processed trilayer light-emitting device architecture, comprising two hydrophobic and mobile-ion-containing "transport layers" sandwiching a hydrophilic and ion-free "intermediate layer", which allows for lowered self-absorption, minimized electrode quenching, and tunable light emission. Our results reveal that the transport layers can be doped in situ when a voltage is applied, that the intermediate layer as desired can contribute significantly to the light emission, and that the key to a successful operation is the employment of a porous and ($\sim$5–10 nm) thin intermediate layer allowing for facile ion transport. We report that such a solution-processed device, comprising a thick trilayer material ($\sim$250 nm) and air-stable electrodes, emits blue light (λ_{peak} = 450, 484 nm) with high efficiency (5.3 cd/A) at a low drive voltage of 5 V.
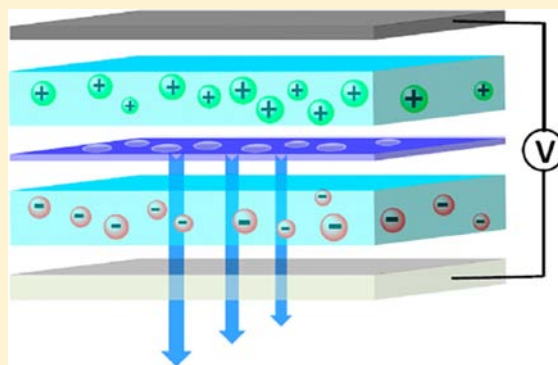
1. INTRODUCTION

The static p−n junction doping structure has for several decades been a highly exploited feature in a wide range of ubiquitous optoelectronic devices, for example, light-emitting diodes (LEDs)[1−3] and organic LEDs (OLEDs).[4−8] The composition and features of this static p−n junction are defined during the device fabrication (typically executed under high vacuum). In contrast, the dynamic formation of a p−n junction structure within the active layer of an electronic device is a more recent invention, which exhibits a structure that is defined in situ during a redistribution of mobile ions within a soft organic semiconductor under the action of an applied voltage.[9−25]

This latter dynamic approach is the basis of operation of light-emitting electrochemical cells (LECs), comprising a single-layer blend of a conjugated polymer (CP) and an electrolyte as the active layer. When a sufficiently high voltage is applied to the electrodes of an LEC ($V \geq E_g/e$; where the latter term is the band gap potential of the CP), the mobile ions redistribute to allow for efficient and balanced bipolar electronic injection and a subsequent doping of the CP, being p-type at the anode and n-type at the cathode. After a turn-on time, a light-emitting p−n junction has formed at the position where the two doped regions made contact.[26−33]

The dynamic p−n junction process is the origin to a number of attractive properties of LECs, notably a high tolerance toward a large, and varying, thickness of the active layer, and the material selection for both electrodes. OLEDs in contrast require a well-defined thickness of the active material constituent(s) and an air-sensitive (low-work function) material

for the cathode/electron-injection layer. As a consequence, a unique opportunity for all-ambient device fabrication using solely solution-processable materials is a much desired, and demonstrated, feature of LECs.[34−37] However, a drawback related to the employment of a thick active layer is that losses due to self-absorption can become prominent and influence the device efficiency in a negative manner. Moreover, it has also become clear that, to allow for increased LEC efficiency and operational lifetime, it is paramount to better understand and control the formation and steady-state structure of the in situ formed p−n junction,[38−42] specifically to ensure its formation in the center of the device to alleviate exciton quenching by the electrodes.[43] Relatively recent studies have also showed that it is highly desirable to keep the p−n junction electrolyte-free during light emission, because performance-detrimental inter-actions between the excitons and immobile and/or remaining electrolyte species otherwise can be prominent.[44−46] Thus, it is of interest to design and develop LEC device structures in which the (majority of the) active layer is effectively transparent to the light emission, where the emission zone is well separated from the electrodes, and where the interactions between the excitons in the emission zone and the electrolyte (mobile ions and ionic solvent) are minimized.

Here, we introduce a trilayer device structure, comprising two hydrophobic {CP + electrolyte} transport layers sandwiching a hydrophilic zwitterionic conjugated polymer (ZP) intermediate layer, with the ZP being free from mobile

ions in its pristine state. We show that such an optimized trilayer structure comprising a porous and (5−10 nm) thin intermediate ZP layer can exhibit a low turn-on voltage for blue light emission and high efficiency, despite the employment of air-stable electrode materials and a significant total (250 nm) thickness for the trilayer active material. We demonstrate that one key to the promising performance is the facile transport of mobile ions through the thin and porous ZP layer and the resulting electrochemical doping of the CP layers next to the electrode surfaces during the turn-on process.

2. EXPERIMENTAL SECTION

The ZP, poly[(9,9-bis((*N*-(4-sulfonate-1-butyl)-*N,N*-dimethylammo-nium)-ethanyl)-2,7-fluorene)-*alt*-2,7-(9,9-dioctylfluorene)], was synthesized using a standard Pd-mediated Suzuki coupling polymerization of the monomers 2,7-dibromo-9,9-bis((*N,N*-dimethylamino)ethanyl)-fluorene and 2,7-bis-(1,3,2-dioxaborolan-2-yl)-9,9-dioctylfluorene; the resulting neutral tertiary amine polymer was quaternized using 1,4-butane sulfone. More details on the synthesis of the ZP are available in the literature.[47] The CP, a blue-emitting polyspirobifluorene-based copolymer (Merck, catalogue number SPB-02T), the salt $LiCF_3SO_3$ (Aldrich), and the ionic solvent/transport material trimethylolpropane ethoxylate (TMPE, M_w = 450 g/mol, Aldrich) were all used as received. The chemical structures of the ZP, the CP, and the electrolyte are displayed in Figure 1a.

For the device fabrication, poly(3,4-ethylenedioxythiophene)-poly-(styrene sulfonate) (PEDOT-PSS, Clevios P VP AI 4083, Heraeus) was spin coated on top of a carefully cleaned indium−tin−oxide (ITO)-coated glass substrate (1.5 × 1.5 cm², 20 ohms/square, Thin Film Devices) at 4000 rpm for 60 s, and the resulting 40 nm thick film
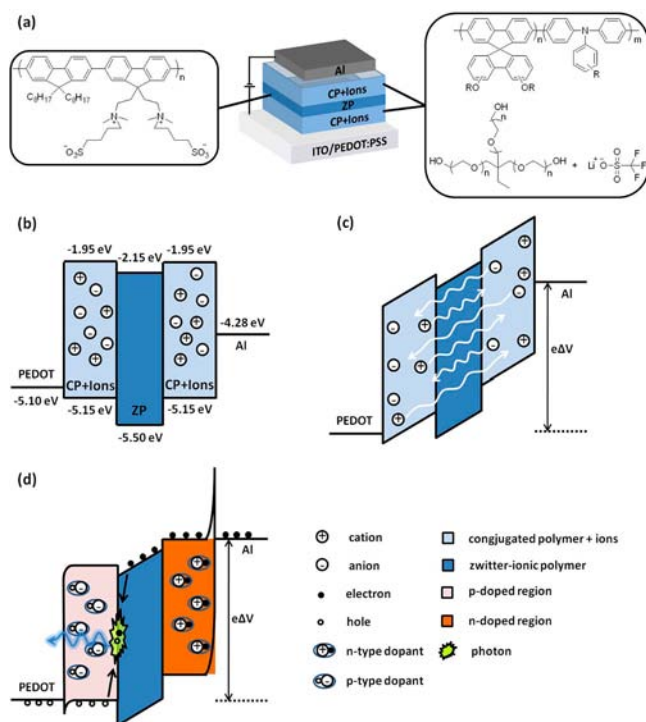

Figure 1. (a) Schematic configuration of the trilayer device, highlighting the chemical structure of the constituents of the active layer. (b) The energy-level diagram of a pristine trilayer device at open circuit, as estimated by cyclic voltammetry. (c) The anticipated initial drift of ions through the intermediate ZP layer following the application of a voltage. (d) The steady-state p−n junction structure with the emission zone pinned at the interface of the intermediate ZP layer.

was dried at T = 120 °C for 6 h. The first transport layer, comprising $\{CP:TMPE:LiCF_3SO_3\}$ in a mass ratio of $\{1:0.1:0.03\}$, was spin-coated from a 10 mg/mL THF solution on top of the PEDOT-PSS layer. The ZP was dissolved in methanol and spin-coated on top of the transport layer at 2000 rpm for 60 s. The ZP concentration was 1 mg/mL for a 6 nm thick layer, 2.5 mg/mL for a 20 nm thick layer, and 5 mg/mL for a 35 nm thick layer. The second and topmost transport layer was thereafter spin-coated on top of the ZP layer, using the same parameters as for the first layer. The thickness of each of the two transport layers in the trilayer structure was measured to be 120 nm. The LEC device structure was finally capped off by thermally evaporating a set of four Al top cathodes (thickness, 100 nm; area, 0.85 × 0.15 cm²) on top of the trilayer active material under a vacuum of <2 × 10⁻⁶ mbar. A schematic of the device structure is presented in Figure 1a. All of the above device preparation steps, except the cleaning of the substrates and the deposition of PEDOT-PSS, were carried out in two interconnected N₂-filled glove boxes ([O₂] < 3 ppm, [H₂O] < 0.5 ppm).

The device characterization was executed in an optical-access vacuum system at a pressure of $p < 1 \times 10^{-5}$ mbar. For the voltage−ramp measurements, the devices were driven by a Keithley 2400 source-meter unit, while the galvanostatic (constant current) and electroluminescence (EL) measurements were driven by an Agilent 2722A source-measure unit. The brightness was detected with a calibrated photodiode equipped with an eye response filter (Hamamatsu Photonics). The EL measurements used a fiber-optic spectrometer (USB2000, Ocean Optics) and were carried out in the N₂-filled glovebox.

Atomic force microscopy (AFM, MultiMode SPM microscope equipped with a Nanoscope IV Controller, Veeco Metrology) was utilized for the measurements of the film thickness and the surface morphology, and contact angle measurements (Biolin Scientific) were performed for the establishment of the hydrophobicity of the different surfaces. Cyclic voltammetry (CV) was employed for the estimation of the electronic structure of the active layer constituents. The CV sweeps were driven and measured by an Autolab PGSTAT302 potentiostat. CP- and ZP-coated Au were used as the working electrode, a Pt wire was used as the counter electrode, and a Ag wire was used as the pseudoreference electrode. The electrolyte was 0.1 M tetrabutylammonium hexafluorophosphate in CH_3CN. Directly after each CV scan, a calibration scan was run with a small amount of ferrocene (Fc) added to the electrolyte for the establishment of CV potentials vs the Fc/Fc⁺ redox couple. The onset potentials for oxidation and reduction were calculated as the intersection of the baseline current with the tangent of the current at the half-maximum of its peak. The CV sample preparation and measurements were carried out in the N₂-filled glovebox.

3. RESULTS AND DISCUSSION

Figure 1a presents the desired configuration of our LEC device and the chemical structures of the constituents in the trilayer active material. Two (light blue) "transport layers", comprising a blend of the CP and mobile Li⁺ and $CF_3SO_3^-$ ions dissolved by TMPE, sandwich a (dark blue) mobile-ion-free "inter-mediate layer" comprising the ZP. The electronic structure of the trilayer device at open-circuit is depicted in Figure 1b, and it is clear that a large barrier for electron injection from the Al cathode into the (right) transport layer exists at this point. Figure 1c illustrates the anticipated initial ionic redistribution following the application of an external voltage (ΔV), and it is notable that the mobile cations and anions from the transport layers are postulated to be able to penetrate and pass through the intermediate layer in a facile manner; we will return to this important topic later on. The accumulation of noncompensated ions next to the electrode interfaces, with its concomitant buildup of a large and local electric field, will eventually allow for efficient and balanced electron and hole injection. The first

injected electronic charge carriers will induce a compensating ionic redistribution and electrochemical doping of the CP, being p-type at the anode and n-type at the cathode. Figure 1d presents the anticipated steady-state p−n junction structure, where the doping regions have grown to encompass almost the entire width of the thick transport layers, while the light emission is primarily confined to the close vicinity of the ZP layer. The n-type/p-type doping renders the transport layers highly conductive for electron/hole transport, which has the attractive consequences that facile injection is possible from any electrode material independent of its work function (and concomitant injection barrier) and that the voltage drop over the transport layers is relatively insignificant.

The realization of a multilayer active material structure using a sequential solution-based fabrication process (here, spin coating) is in our employed approach hinging on a distinctly different solubility of the neighboring layers, here, manifested in a measured water contact angle of 100° for a sole transport layer on a glass substrate and 75° for a sole ZP layer on a glass substrate (data not shown). In other words, for this approach to work, the solvent utilized for the layer to be deposited should not dissolve or remove the underlying layer. Figure 2 presents
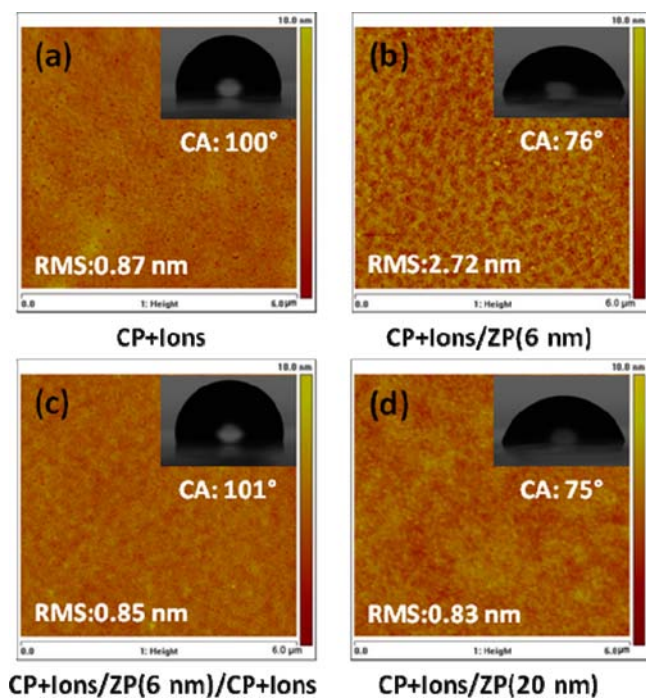
Figure 2. AFM surface morphology (6 × 6 μm) maps and water contact angle photographs (inset) executed on the upper surface of the following layered samples (with the upper-most surface positioned to the right): (a) {CP+ions} (d = 120 nm) single-layer, (b) {CP+ions} (d = 120 nm)/ZP (d = 6 nm) bilayer, (c) {CP+ions} (d = 120 nm)/ZP (d = 6 nm)/{CP+ions} (d = 120 nm) trilayer, and (d) {CP+ions} (d = 120 nm)/ZP (d = 20 nm) bilayer.

AFM micrographs and photographs of water contact angle measurements (see inset) recorded during the sequential deposition of the constituent layers in the trilayer structure. The contact angle data show that both the bottom layer (a) and the top layer (c) exhibit the characteristic hydrophobic signature of a pristine transport layer (a large water contact angle of 100−101°), while a thin and thick version of the intermediate layer (b and d, respectively) both exhibit the

characteristic hydrophilic nature of the ZP layer (a water contact angle of 75−76°). The water contact angle measurements thus yield support for that the trilayer structure indeed has been attained.

The AFM data reveal a smooth surface for both the bottom and the top transport layers (a and c), as quantified by a root-mean-square (rms) roughness value of 0.85−0.87 nm, while the surface of the thin ZP intermediate layer (b) is distinctly more uneven, with an rms value of 2.72 nm. The latter is particularly interesting in the context of that the total average thickness of the thin intermediate layer is a mere 6 nm, which implies a porous character for this thin intermediate layer in the trilayer structure.

We have also fabricated and characterized trilayer structures with a thicker intermediate ZP layer (thickness = 20 and 35 nm), and Figure 2d presents data recorded on a 20 nm-thick intermediate layer deposited on top of a transport layer. As noted above, the thicker intermediate layers exhibit essentially the same water contact angle as the thin intermediate layer, but in contrast to the thin layer display a smooth surface, with an rms value of 0.83 nm for the 20 nm-thick intermediate layer as compared to 2.72 nm for the 6 nm-thick intermediate layer (compare Figure 2d with Figure 2b). This observation implies that a critical lower value for the thickness of the intermediate ZP layer exists, below which it exhibits a rough surface and pronounced porous character when deposited on top of a transport layer.

The influence of the thickness of the intermediate ZP layer on the optoelectronic performance of a trilayer LEC device is found to be significant, despite the fact that the total thickness of the active layer is dominated by the two transport layers with a combined thickness of 240 nm. Figure 3a reveals the turn-on
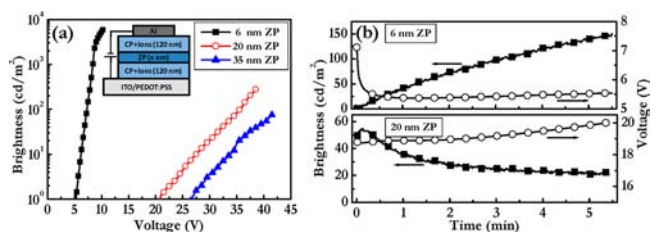
Figure 3. (a) Brightness−voltage characteristics as a function of the thickness of the intermediate ZP layer in a trilayer device, with the device structure and the thickness being identified in the two insets. The scan rate was 0.1 V/s. (b) The turn-on kinetics of a trilayer device with a thickness for the intermediate ZP layer of 6 nm (top panel) and 20 nm (bottom panel). Both devices were driven in galvanostatic mode at j = 7.7 mA/cm^2.

voltage and maximum brightness as a function of ZP thickness; while the 6 nm-thin ZP trilayer device demonstrates a low turn-on voltage (defined to be the voltage at which the brightness exceeds 1 cd/m^2) of 5.0 V and a high maximum brightness of 6200 cd/m^2 at 10.4 V, the thicker-intermediate-layer trilayer devices (ZP thickness: 20/35 nm) exhibit an inferior performance in the form of a significantly higher turn-on-voltage (20/27 V) and a lower maximum brightness (280/75 cd/m^2). The classical signatures of LEC operation are a low turn-on voltage independent of the thickness of the active layer and the material selection for the electrodes, and an increasing brightness and a decreasing voltage (during galvanostatic operation at a set current) with time. These identifying LEC features could indeed be observed for 6 nm-thin ZP trilayer

devices, as evidenced by the turn-on behavior in Figure 3a and the temporal optoelectronic response in the top panel of Figure 3b. In contrast, the trilayer devices comprising a thicker intermediate ZP layer did not exhibit any of the characteristic LEC features, as indicated by the high turn-on voltage in Figure 3a, and the decreasing brightness and increasing voltage with time for the 20 nm-thin device presented in the bottom panel of Figure 3b. The trilayer LEC with an intermediate ZP layer thickness of 35 nm exhibited the same qualitative behavior as the trilayer device with a ZP thickness of 20 nm. Thus, it was solely the trilayer device featuring a 6 nm thin intermediate layer that was found to function as an LEC.

An interesting question then emerges: What is the cause for the profound dependence of the device performance on the thickness of the intermediate ZP layer? Or more specifically stated: Why does the trilayer LEC with a 6 nm thick intermediate layer exhibit good performance, while the devices featuring thicker intermediate layers fail miserably? We propose that the answer is directly traceable to the observed relationship between the thickness and porosity of the intermediate layer (see Figure 2 and related text) and the employed $LiCF_3SO_3-$ TMPE electrolyte.[45] A thin and porous intermediate layer will allow for facile ion passage and a concomitant bulk ionic redistribution, which are the prerequisites for successful LEC operation, as schematically outlined in Figure 1b−d. In contrast, when the intermediate layer is highly dense and not prone to transport of bulky $CF_3SO_3^-$ anions and Li$^+$−TMPE cationic coordination complexes, it will act as an effective ion-blocking layer. In such an ion-blocking scenario, the mobile ions will not be able to reach and accumulate at the electrode interfaces, which will prohibit the LEC function and the in situ p−n junction formation. For our specific device configuration, we also anticipate that the trilayer device void of LEC function will exhibit a nonbalanced electron/hole injection due to the much larger barrier for electron injection over hole injection (see Figure 1b). We note that this hypothesis is supported by a lower measured maximum efficiency for the 20 nm-thick devices in comparison to the 6 nm-thin device under identical galvanostatic drive conditions ($j = 7.7$ mA/cm^2): 0.71 cd/A and 0.12 lm/W (at 55 cd/m^2) versus 5.3 cd/A and 2.7 lm/W (at 410 cd/m^2).

We now turn our attention to the anticipated and measured electroluminescence (EL) from the trilayer LEC. The electronic structure suggests that holes and electrons will be blocked in their forward motion at opposite sides of the interface between the p-type doped CP and the ZP, thus localizing the exciton formation to this interface (see Figure 1d). The EL should as a consequence exhibit a bimolecular exciplex character,[48−51] which is different from the EL spectrum from that of the pristine ZP and CP. To test this hypothesis, we present in Figure 4 the EL spectrum from three different LECs: a single-layer LEC comprising the "transport-layer" CP as the emitter, a single-layer LEC comprising the "intermediate-layer" ZP as the emitter, and a trilayer LEC comprising a 6 nm-thin ZP as the intermediate layer. The single-layer CP LEC (green ●) displays the narrowest and most symmetric EL spectrum with a dominant peak positioned at 480 nm, while the EL spectrum from the single-layer ZP LEC (blue △) is much broader with two distinct peaks located at 435 nm (major) and 494 nm (minor). The EL spectrum from the trilayer device (■) is markedly different from both single-layer devices, with two well-resolved peaks at 450 nm (minor) and 484 nm (major). In this context, we call particular attention to that the CP by
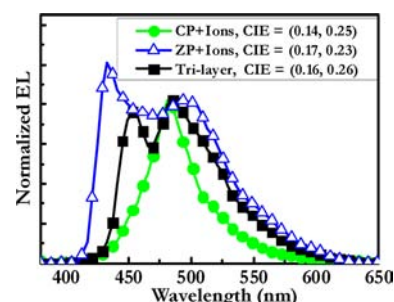
Figure 4. Normalized EL spectra from three different LECs: (i) A single-layer device comprising the CP blended with an {TMPE:-LiCF$_3$SO$_3$} electrolyte as the active layer with a thickness of 120 nm. (ii) A single-layer device comprising the ZP blended with an {PEO:KCF$_3$SO$_3$} electrolyte as the active layer with a thickness of 90 nm. (iii) A trilayer device with a 6 nm-thick intermediate ZP layer. Note that all three EL spectra have been normalized to their respective EL peak at ∼500 nm for clarity. The corresponding CIE coordinates are included in the inset.

volume dominates the ZP in the trilayer device by a factor of 40, but that the EL from the trilayer device nevertheless bears no clear resemblance of the single-layer CP LEC. With this information at hand, we find it established that the emission zone in the trilayer LEC is encompassing (parts of) the thin intermediate ZP layer, and that the concept of an exciplex emission stemming from the interface between the anodic transport layer and the intermediate ZP layer indeed is plausible. We also note that a consequence of this finding is that the doping on both sides of the intermediate ZP should be relatively symmetric, that is, that the average doping concentration level in both transport layers is essentially identical, as the thickness of both layers is identical and the redox balance requires each p-type doping event to be matched by a corresponding n-type doping event (barring the existence of side-reaction events).[44] We also mention that we have systematically studied the EL from single-layer devices with different active-material thickness to exclude that the observed shifts in the EL spectra stem from optical-outcoupling effects. Some of these results are presented in the Supporting Information.

One of our main motivations for assembling and investigating multilayer LEC structures was to minimize the anticipated significant self-absorption of the exiting photons during their passage through the doped regions, which will be particularly high in devices featuring practical thick active layers, and to eliminate electrode-induced exciton quenching reactions. In this context, it is satisfying to report that the 250 nm-thick trilayer structure with an intermediate ZP layer thickness of 6 nm exhibited a higher quantum efficiency (5.3 cd/A) than single-layer devices comprising the ZP (0.46 cd/A; active layer thickness = 100 nm) or the conjugated polymer CP (3.5 cd/A; active layer thickness = 230 nm) as the sole emitter, under identical operational conditions. Experimental data for the CP-LEC, as well as for two bilayer devices, are presented in the Supporting Information. However, it should be pointed out that our employed trilayer structure is far from ideal from a minimized self-absorption viewpoint, because the bandgap of the ZP actually is larger than the bandgap of the CP residing in the transport layers (see Figure 1b). Thus, it is advisable to direct future work in this field toward the synthesis of ZPs with a smaller band gap to more appropriately tune the light emission and to attain even higher efficiency values.

We also note that the finding that a porous intermediate layer can be a necessity for the attainment of electrochemical doping in trilayer device structures could have implications for earlier work carried out by the research groups of Bazan,[52−56] Nguyen,[52,53,57,58] and Cao.[59−61] These authors investigated multilayer device architectures with "injection layers" comprising a conjugated polyelectrolyte, with pendant ionic groups and mobile counterions, sandwiching an ion-free conjugated polymer. A key question originating from their work was whether the mobile ions in the injection layers could redistribute and allow for electrochemical doping of the ion-free conjugated-polymer layer. Although one should exercise caution in exporting conclusions from one device system to another with potentially markedly different properties, specifically the effective ion size and intrinsic capacity for ion transport of "our" ZP in comparison to "their" CP, we note that a study on the dependence of the thickness and porosity of the intermediate layer could possibly shed light on the interesting and important question whether electrochemical doping can take place also in such systems.

4. CONCLUSIONS

We present a solution-processed trilayer light-emitting device architecture, comprising two hydrophobic transport layers sandwiching a hydrophilic zwitterionic conjugated-polymer intermediate layer. We show that mobile ions residing in the conjugated polymer-based transport layers can redistribute and allow for electrochemical doping following the application of an external voltage, provided that the intermediate layer is thin and porous. The light emission from such appropriately designed devices is demonstrated to originate from a close proximity of the thin intermediate layer, despite that the latter constitutes only a mere 2.5% of the total active material volume. This observation points out a path toward a facile tuning of the light emission, spatial localization of excitons formation, and a concomitant minimization of losses due to self-absorption and electrode quenching, for such solution-processed trilayer devices comprising thick active layers and air-stable electrodes.

■ ASSOCIATED CONTENT

Ⓢ Supporting Information

Device data for single-layer and bilayer devices as well as the EL spectra for single-layer CP devices with varying thickness. This material is available free of charge via the Internet at http://pubs.acs.org.

■ AUTHOR INFORMATION

Corresponding Author
ludvig.edman@physics.umu.se

Notes
The authors declare no competing financial interest.

■ ACKNOWLEDGMENTS

■ REFERENCES

(1) Nick Holonyak, J.; Bevacqua, S. F. *Appl. Phys. Lett.* **1962**, *1*, 82−83.

(2) Krames, M. R.; Ochiai-Holcomb, M.; Hofler, G. E.; Carter-Coman, C.; Chen, E. I.; Tan, I.-H.; Grillot, P.; Gardner, N. F.; Chui, H. C.; Huang, J.-W.; Stockman, S. A.; Kish, F. A.; Craford, M. G.; Tan, T. S.; Kocot, C. P.; Hueschen, M.; Posselt, J.; Loh, B.; Sasser, G.; Collins, D. *Appl. Phys. Lett.* **1999**, *75*, 2365−2367.

(3) Vispute, R. D.; Talyansky, V.; Choopun, S.; Sharma, R. P.; Venkatesan, T.; He, M.; Tang, X.; Halpern, J. B.; Spencer, M. G.; Li, Y. X.; Salamanca-Riba, L. G.; Iliadis, A. A.; Jones, K. A. *Appl. Phys. Lett.* **1998**, *73*, 348−350.

(4) Tang, C. W.; VanSlyke, S. A. *Appl. Phys. Lett.* **1987**, *51*, 913−915.

(5) Tang, C. W.; VanSlyke, S. A.; Chen, C. H. *J. Appl. Phys.* **1989**, *65*, 3610−3616.

(6) Baldo, M. A.; O'Brien, D. F.; You, Y.; Shoustikov, A.; Sibley, S.; Thompson, M. E.; Forrest, S. R. *Nature* **1998**, *395*, 151−154.

(7) Reineke, S.; Lindner, F.; Schwartz, G.; Seidler, N.; Walzer, K.; Lussem, B.; Leo, K. *Nature* **2009**, *459*, 234−238.

(8) Sun, Y.; Giebink, N. C.; Kanno, H.; Ma, B.; Thompson, M. E.; Forrest, S. R. *Nature* **2006**, *440*, 908−912.

(9) Zhou, L. X.; Liu, S. J.; Zhao, Q.; Ling, Q. D.; Huang, W. *Prog. Chem.* **2011**, *23*, 1871−1882.

(10) Costa, R. D.; Orti, E.; Bolink, H. J. *Pure Appl. Chem.* **2011**, *83*, 2115−2128.

(11) Liu, J.; Engquist, I.; Crispin, X.; Berggren, M. *J. Am. Chem. Soc.* **2012**, *134*, 901−904.

(12) Pei, Q. B.; Yu, G.; Zhang, C.; Yang, Y.; Heeger, A. J. *Science* **1995**, *269*, 1086−1088.

(13) Pei, Q. B.; Yang, Y.; Yu, G.; Zhang, C.; Heeger, A. J. *J. Am. Chem. Soc.* **1996**, *118*, 3922−3929.

(14) Edman, L. *Electrochim. Acta* **2005**, *50*, 3878−3885.

(15) Inganas, O. *Chem. Soc. Rev.* **2010**, *39*, 2633−2642.

(16) Leger, J. M. *Adv. Mater.* **2008**, *20*, 837−841.

(17) Matyba, P.; Maturova, K.; Kemerink, M.; Robinson, N. D.; Edman, L. *Nat. Mater.* **2009**, *8*, 672−676.

(18) Matyba, P.; Yamaguchi, H.; Eda, G.; Chhowalla, M.; Edman, L.; Robinson, N. D. *ACS Nano* **2010**, *4*, 637−642.

(19) Sun, Q.; Li, Y.; Pei, Q. *J. Disp. Technol.* **2007**, *3*, 211−224.

(20) deMello, J. C.; Halls, J. J. M.; Graham, S. C.; Tessler, N.; Friend, R. H. *Phys. Rev. Lett.* **2000**, *85*, 421−424.

(21) Hu, T.; He, L.; Duan, L.; Qiu, Y. *J. Mater. Chem.* **2012**, *22*, 4206−4215.

(22) Dumur, F.; Bertin, D.; Gigmes, D. *Int. J. Nanotechnol.* **2012**, *9*, 377−395.

(23) Tordera, D.; Meier, S.; Lenes, M.; Costa, R. D.; Orti, E.; Sarfert, W.; Bolink, H. J. *Adv. Mater.* **2012**, *24*, 897−900.

(24) Mills, T. J.; Lonergan, M. C. *Phys. Rev. B* **2012**, *85*, 035203.

(25) Georgiadou, D. G.; Palilis, L. C.; Vasilopoulou, M.; Pistolis, G.; Dimotikali, D.; Argitis, P. *J. Mater. Chem.* **2011**, *21*, 9296−9301.

(26) Gao, J.; Dane, J. *J. Appl. Phys.* **2005**, *98*, 063513.

(27) Hu, Y.; Gao, J. *J. Am. Chem. Soc.* **2009**, *131*, 18236−18237.

(28) Shin, J. H.; Dzwilewski, A.; Iwasiewicz, A.; Xiao, S.; Fransson, A.; Ankah, G. N.; Edman, L. *Appl. Phys. Lett.* **2006**, *89*, 013509.

(29) Shin, J. H.; Edman, L. *J. Am. Chem. Soc.* **2006**, *128*, 15568−15569.

(30) Matyba, P.; Andersson, M. R.; Edman, L. *Org. Electron.* **2008**, *9*, 699−710.

(31) Toshner, S. B.; Zhu, Z. H.; Kosilkin, I. V.; Leger, J. M. *ACS Appl. Mater. Interfaces* **2012**, *4*, 1149−1153.

(32) Hu, Y. F.; Dorin, B.; Teng, F.; Gao, J. *Org. Electron.* **2012**, *13*, 361−365.

(33) van Reenen, S.; Matyba, P.; Dzwilewski, A.; Janssen, R. A. J.; Edman, L.; Kemerink, M. *J. Am. Chem. Soc.* **2010**, *132*, 13776−13781.

(34) Burnett, K. O.; Crooker, P. P.; Haegel, N. M.; Yoshioka, Y.; MacKenzie, D. *Synth. Met.* **2011**, *161*, 1496−1499.

(35) Matyba, P.; Yamaguchi, H.; Chhowalla, M.; Robinson, N. D.; Edman, L. *ACS Nano* **2011**, *5*, 574−580.

(36) Yu, Z.; Liu, Z.; Wang, M.; Sun, M.; Lei, G.; Pei, Q. *J. Photonics Energy* **2011**, *1*, 011003−15.

(37) Yu, Z. B.; Niu, X. F.; Liu, Z. T.; Pei, Q. B. *Adv. Mater.* **2011**, *23*, 3989−3994.

(38) Fang, J.; Matyba, P.; Edman, L. *Adv. Funct. Mater.* **2009**, *19*, 2671−2676.

(39) Sandstrom, A.; Matyba, P.; Edman, L. *Appl. Phys. Lett.* **2010**, *96*, 053303.

(40) Shao, Y.; Bazan, G. C.; Heeger, A. J. *Adv. Mater.* **2007**, *19*, 365−370.

(41) Tang, S.; Pan, J.; Buchholz, H.; Edman, L. *ACS Appl. Mater. Interfaces* **2011**, *3*, 3384−3388.

(42) Yu, Z.; Wang, M.; Lei, G.; Liu, J.; Li, L.; Pei, Q. *J. Phys. Chem. Lett.* **2011**, *2*, 367−372.

(43) Burin, A. L.; Ratner, M. A. *J. Phys. Chem. A* **2000**, *104*, 4704−4710.

(44) Fang, J.; Matyba, P.; Robinson, N. D.; Edman, L. *J. Am. Chem. Soc.* **2008**, *130*, 4562−4568.

(45) Tang, S.; Edman, L. *J. Phys. Chem. Lett.* **2010**, *1*, 2727−2732.

(46) Wågberg, T.; Hania, P. R.; Robinson, N. D.; Shin, J. H.; Matyba, P.; Edman, L. *Adv. Mater.* **2008**, *20*, 1744−1746.

(47) Fang, J.; Wallikewitz, B. H.; Gao, F.; Tu, G.; Müller, C.; Pace, G.; Friend, R. H.; Huck, W. T. S. *J. Am. Chem. Soc.* **2011**, *133*, 683−685.

(48) Berggren, M.; Gustafsson, G.; Inganas, O.; Andersson, M. R.; Hjertberg, T.; Wennerstrom, O. *J. Appl. Phys.* **1994**, *76*, 7530−7534.

(49) Osaheni, J. A.; Jenekhe, S. A. *Macromolecules* **1994**, *27*, 739−742.

(50) Chao, C.-I.; Chen, S.-A. *Appl. Phys. Lett.* **1998**, *73*, 426−428.

(51) Goushi, K.; Yoshida, K.; Sato, K.; Adachi, C. *Nat. Photonics* **2012**, *6*, 253−258.

(52) Hoven, C. V.; Garcia, A.; Bazan, G. C.; Nguyen, T.-Q. *Adv. Mater.* **2008**, *20*, 3793−3810.

(53) Hoven, C.; Yang, R.; Garcia, A.; Heeger, A. J.; Nguyen, T.-Q.; Bazan, G. C. *J. Am. Chem. Soc.* **2007**, *129*, 10976−10977.

(54) Li, H.; Xu, Y.; Hoven, C. V.; Li, C.; Seo, J. H.; Bazan, G. C. *J. Am. Chem. Soc.* **2009**, *131*, 8903−8912.

(55) Yang, R.; Wu, H.; Cao, Y.; Bazan, G. C. *J. Am. Chem. Soc.* **2006**, *128*, 14422−14423.

(56) Seo, J. H.; Namdas, E. B.; Gutacker, A.; Heeger, A. J.; Bazan, G. C. *Adv. Funct. Mater.* **2011**, *21*, 3667−3672.

(57) Nguyen, H. T.; Nguyen, T. Q.; Nguyen, M. T. *Chem. Phys. Lett.* **2012**, *530*, 39−44.

(58) Garcia, A.; Bakus, R. C.; Zalar, P.; Hoven, C. V.; Brzezinski, J. Z.; Nguyen, T. Q. *J. Am. Chem. Soc.* **2011**, *133*, 2492−2498.

(59) Wu, H.; Huang, F.; Mo, Y.; Yang, W.; Wang, D.; Peng, J.; Cao, Y. *Adv. Mater.* **2004**, *16*, 1826−1830.

(60) Huang, F.; Wu, H.; Wang, D.; Yang, W.; Cao, Y. *Chem. Mater.* **2004**, *16*, 708−716.

(61) Huang, F.; Wu, H.; Cao, Y. *Chem. Soc. Rev.* **2010**, *39*, 2500−2521.